Identifying hydrodynamic interaction effects in tethered polymers in uniform flow

Diego Kienle,[1,*] Roland Rzehak,[2] and Walter Zimmermann[1]
[1]*Theoretische Physik I, Universität Bayreuth, D-95440 Bayreuth, Germany*
[2]*Forschungszentrum Dresden, D-01328 Dresden, Germany*
(Received 15 December 2010; published 29 June 2011)

Using Brownian dynamics simulations, we investigate how hydrodynamic interaction (HI) affects the behavior of tethered polymers in uniform flow. While it is expected that the HI within the polymer will lead to a dependency of the polymer's drag coefficient on the flow velocity, the interchain HI causes additional screening effects. For the case of two polymers in uniform flow with their tether points a finite distance apart, it is shown that the interchain HI not only causes a further reduction of the drag per polymer with decreasing distance between the tether points but simultaneously induces a polymer-polymer attraction as well. This attraction exhibits a characteristic maximum at intermediate flow velocities when the drag forces are of the order of the entropic forces. The effects uniquely attributed to the presence of HI can be verified experimentally.

DOI: 10.1103/PhysRevE.83.062802 PACS number(s): 82.35.Lr, 05.40.Jc, 47.15.G−, 83.10.Mj

The dynamics of flexible polymers in liquids and the interaction between different sections of the polymer mediated by the fluid, the so-called hydrodynamic interaction (HI), is the origin of a variety of fascinating flow phenomena, such as turbulent drag reduction [1–3], elastic turbulence [4], and the coil-stretch transition predominant in extensional flows [5]. Many experiments have been performed to explore the dynamic interplay between polymers and the fluid by studying the deformation of single polymers in uniform, shear, and extensional flow fields [6–10] as well as their time-periodic dynamics in linear shear and Poiseuille flow [11–16].

A key question in exploring polymer-fluid interaction is to find suitable experimental setups as well as appropriate measurable quantities which allow to attribute the observed behavior to HI effects in a unique manner. It is known that hydrodynamic screening affects the elongation R_{ee} of tethered polymers in uniform flows and depends on the flow velocity u_{ext} in a nonlinear manner in general. However, such nonlinear dependency of R_{ee} on the flow velocity is already observed for free-draining polymers in the absence of HI [6,17–22].

In this Brief Report, we use the drag force acting on the polymer instead of its elongation as a means to probe in *uniform* flows the HI effects in a unique manner, which we calculate through Brownian dynamics (BD) simulations of bead-spring models. After a brief introduction of the polymer model, we start from the case of a single tethered polymer and show that screening effects within the polymer appear through the velocity dependency of the drag coefficient $\zeta = \zeta(\mathbf{u}_{\mathrm{ext}})$, in agreement with earlier studies where an effective Stokes radius was used to characterize the presence of intrachain HI [23,24]. Beyond the single-chain case, it is shown by example of two polymers in uniform flow that the HI between polymers leads to an enhanced drag reduction and, importantly, induces lateral forces, causing an effective polymer-polymer attraction, which is a unique fingerprint of HI as well.

The Brownian dynamics of a system of one or more tethered bead-spring polymers exposed to a uniform flow field is governed by Langevin's equation [19,25]:

$$\dot{\mathbf{R}} = \mathbf{u}_0(\mathbf{R}) + \mathbf{H}\cdot\mathbf{F} + \sqrt{2k_BT\mathbf{H}}\cdot\boldsymbol{\xi}, \tag{1}$$

where $\mathbf{R} = (\mathbf{R}_1, \ldots, \mathbf{R}_{(M\times N)})$ describes the conformation of the M polymers, each consisting of N beads. $\mathbf{u}_0(\mathbf{R})$ represents the external unperturbed flow field at the bead positions, k_B is Boltzmann's constant, and T is the temperature. The matrix square root of the mobility matrix $\mathbf{H}$ appearing in Eq. (1) is numerically calculated by means of Tschebyscheff polynomials, as described in Refs. [20,26]. $\boldsymbol{\xi}(t)$ is an uncorrelated Gaussian white noise whose components ξ_i have zero mean $\langle\xi_i(t)\rangle = 0$ and unit variance $\langle\xi_i(t)\xi_j(t')\rangle = \delta(t-t')\delta_{ij}$, with $i,j \in x,y,z$. $\mathbf{F}$ refers to all potential forces and includes the excluded-volume interactions (EVI) among the beads described by a Lennard-Jones potential and the next-neighbor bond forces between beads on the same polymer, which are modeled here by a finite extensible nonlinear elastic (FENE) potential [27,28]. All distances are given in units of the bond length, with $b \approx 0.96$ in the FENE model [20]. The hydrodynamic interaction between two beads i and j, which may belong to the same or to different polymer chains, is described by the Rotne-Prager tensor [2,29]. In the region where the beads do not overlap, i.e., $r_{ij} = \left|\mathbf{R}_i - \mathbf{R}_j\right| \geqslant 2a$ $(i \neq j)$, its off-diagonal elements are determined by [29]

$$\mathbf{H}_{ij} = \frac{3}{4\zeta_s}\frac{a}{r_{ij}}\left[\left(1-\frac{2a^2}{r_{ij}^2}\right)\left(\mathbf{I}+\hat{\mathbf{r}}_{ij}\otimes\hat{\mathbf{r}}_{ij}\right)+\frac{8a^2}{3r_{ij}^2}\mathbf{I}\right] \tag{2}$$

and is extended to the overlap region $r_{ij} < 2a$ by

$$\mathbf{H}_{ij} = \frac{1}{\zeta_s}\left[\left(1-\frac{9}{32}\frac{r_{ij}}{a}\right)\mathbf{I}+\frac{3}{32}\frac{r_{ij}}{a}\hat{\mathbf{r}}_{ij}\otimes\hat{\mathbf{r}}_{ij}\right]. \tag{3}$$

The diagonal elements of the mobility tensor $\mathbf{H}$ are just the inverse of the drag coefficient ζ_s for a single bead, i.e., $\mathbf{H}_{ii} = \mathbf{I}/\zeta_s$. In the limit $a/r_{ij} \to 0$, the nondiagonal elements of $\mathbf{H}_{ij}$ vanish, and one approaches the free-draining (no HI) limit, in which case the mobility matrix of the entire system is determined only by ζ_s and does not depend on the polymer conformation. Throughout this work, we use $N = 100$ beads per chain and a bead radius given by $a = \zeta_s/6\pi\eta$, with ζ_s

*Corresponding author: diego.kienle@uni-bayreuth.de

being the Stokes friction coefficient of a single isolated bead. η refers to the viscosity of the solvent. All other parameters appearing in forces and so on are chosen as in Refs. [20,28]. In all plots, we use the normalized velocity $u_{\rm ext}/u_{\rm ref}$, where we define the reference velocity $u_{\rm ref}$ as follows: employing the Pincus relation for a blob with Flory radius $R_F = bN^{1/2}$ and bond length b, we obtain the balance between the drag and entropic force, i.e., $6\pi\eta R_F \tilde{u}_{\rm ref} = k_BT/R_F$ [1]. Note that for large N the ratio k_BT/R_F and thus $\tilde{u}_{\rm ref}$ are quite small. To eliminate this N dependence, we multiply $\tilde{u}_{\rm ref}$ by the number of segments, so that $u_{\rm ref} := k_BTN/6\pi\eta R_F^2 = k_BT/6\pi\eta b^2$.

The form of the mobility matrix $\mathbf{H}_{ij}$ in Eqs. (2) and (3) implies that the hydrodynamic screening of the local flow field and the reduction of the drag force on each bead depend not only on the distance r_{ij} between the beads but also on the orientation of $\mathbf{r}_{ij}$ relative to the flow direction. This can be illustrated by a simple example of a two-bead system. With $\mathbf{r}_{12}$ either parallel ($\parallel$) or perpendicular ($\perp$) to the external flow $\mathbf{u}_{\rm ext} = u_{\rm ext}\hat{e}_x$, the drag forces $\mathbf{F}^{\parallel}$ and $\mathbf{F}^{\perp}$ on each bead are parallel to the flow direction $\hat{e}_x$ and are given by [30]

$$\mathbf{F}^{\parallel} = \frac{\zeta_s u_{\rm ext}}{1+\frac{3a}{2r_{12}}}\hat{e}_x, \qquad \mathbf{F}^{\perp} = \frac{\zeta_s u_{\rm ext}}{1+\frac{3a}{4r_{12}}}\hat{e}_x.$$

Assuming $r_{12} = 2a$, for example, the drag forces on each bead relative to the free-draining limit are $|\mathbf{F}^{\parallel}|/\zeta_s u_{\rm ext} \approx 57\%$ and $|\mathbf{F}^{\perp}|/\zeta_s u_{\rm ext} \approx 72\%$, respectively. If the bead vector $\mathbf{r}_{12}$ is skewly oriented to the flow direction, the drag picks up lateral force components [30], which can lead to an effective attraction between beads or polymers.

As discussed in the introduction, in uniform flows a direct probe of HI effects is possible by determining the drag coefficient ζ of the whole polymer chain, which we define in analogy to the Stokes' law for a rigid sphere [31] through the relation $F_d := \zeta u_{\rm ext}$, with F_d being the *total* drag force acting on the entire polymer and $u_{\rm ext}$ being the uniform flow velocity. An alternative way to probe HI effects is to assign the polymer an effective Stokes radius through $R_p = \zeta/6\pi\eta$ and to look how R_p depends on the polymer extension, as done in previous studies [23,24].

Note that in Stokes' law the drag coefficient ζ is determined by the sphere's geometry through its radius R, i.e., $\zeta = 6\pi\eta R$ [31]. In general, such a relation no longer holds for deformable objects such as polymers, which experience a different drag force depending on the conformational state they adopt for a given velocity $u_{\rm ext}$. Importantly, in the *absence* of HI the *uniformity* of the original flow field is preserved, so that ζ is independent of $u_{\rm ext}$. In this free-draining case, the total drag on the polymer with N beads is simply given by the sum of the drag on each bead, $F_d = N\zeta_s u_{\rm ext}$, irrespective of the polymer extension with a *constant* drag coefficient $\zeta_f = N\zeta_s$. Hence, any velocity dependency of the drag coefficient ζ is a unique signature of HI.

In our BD simulations, F_d is determined from the data by noticing that the total drag force the flow exerts on the tethered polymer is opposite in sign and equals the force that must be applied to hold the polymer in place. This latter force is located at the first bead $\mathbf{R}_1$, which is connected to the tether point by a Hookean spring with force constant κ. Thus, F_d can be easily obtained from the displacement between $\mathbf{R}_1$ and the tether point.

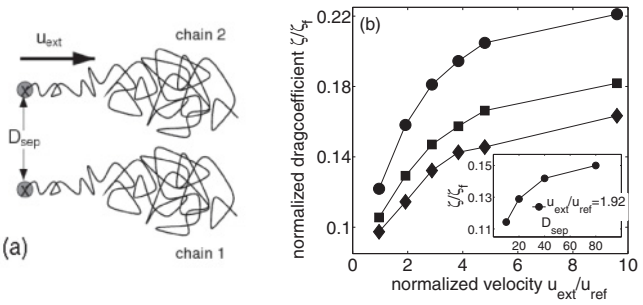

FIG. 1. (a) Two FENE polymers in uniform flow $\mathbf{u}_{\rm ext} = u_{\rm ext}\hat{e}_x$, with their ends tethered at a distance $D_{\rm sep}$. (b) Normalized drag coefficient ζ/ζ_f per polymer as a function of the normalized velocity $u_{\rm ext}/u_{\rm ref}$ for $D_{\rm sep} = 10.0$ (diamonds) and 20.0 (squares) and for a single chain, i.e., $D_{\rm sep} = \infty$ (circles). The inset shows ζ/ζ_f as a function of $D_{\rm sep}$ for $u_{\rm ext}/u_{\rm ref} = 1.92$.

Figure 1(a) illustrates the setup to determine the drag coefficient ζ for a polymer in our simulations. To investigate HI effects not only within a single polymer but also between different polymers, the ends of two polymers are fixed at a variable distance $D_{\rm sep}$ between their tether points, and a uniform flow field $u_{\rm ext}$ is applied. The chains are described by a FENE model including EVI and account for both the intrachain and interchain interaction due to HI. To achieve in BD simulations with $N = 100$ beads for each chain a similar ratio for the drag coefficients in the stretched and coiled conformation $\zeta_{rod}/\zeta_{coil} \sim 2$ as for a 150-μm-long DNA-strand with $N \approx 2000$ Kuhn segments [18], we adjust the ratio between the bead radius a and bond length b to $a/b \sim 0.25$. Figure 1(b) shows the drag coefficient ζ/ζ_f normalized to the drag coefficient $\zeta_f = N\zeta_s$ in the free-draining limit as a function of the normalized velocity $u_{\rm ext}/u_{\rm ref}$ at various separations $D_{\rm sep}$; the statistical errors are quite small, with the magnitude given by the size of the symbols used in Fig. 1(b). In the limit of noninteracting chains ($D_{\rm sep} = \infty$), one obtains the drag coefficient of a single chain, where the drag grows monotonously with increasing flow velocity since the intrachain HI is gradually reduced. However, since in a FENE model the bond length b between nearest-neighbor beads remains nearly fixed, the HI between the beads persists even in the stretched configuration, so that the drag is still only 22% of the drag at free draining. With smaller separation $D_{\rm sep} = 20$ and 10, the interchain becomes significant and leads to a further reduction of the drag ζ/ζ_f [see Fig. 1(b) and in the inset] due to the screening of the flow in between the chains.

The observed velocity dependence of ζ/ζ_f discussed in Fig. 1 originates from the screening due to both the intrachain and interchain HI. However, it is only the *interchain* HI that induces flow-induced *lateral* forces and thus leads to an effective chain attraction, as shown in Fig. 2. To illustrate this effect, we consider two chains whose tether points are separated by $D_{\rm sep} = 10$ and 20, at first neglecting thermal fluctuations [$T = 0$ in Eq. (1)]. A measure for the attraction is given by the difference between $D_{\rm sep}$ and $\Delta y_{\rm com}$, with $\Delta y_{\rm com} := y^1_{\rm com} - y^2_{\rm com}$ being the lateral distance of the center

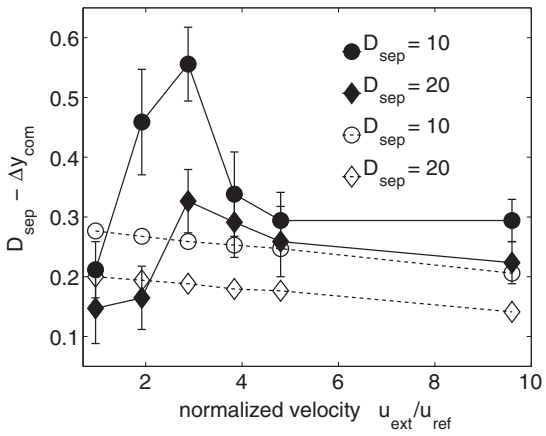

FIG. 2. Difference $D_{\rm sep} - \Delta y_{\rm com}$ between the distance of the tether points and the lateral distance of the centers of mass with $D_{\rm sep} = 10$ and 20 for a FENE chain with the full mobility matrix (solid circles and solid diamonds) and without thermal fluctuations (open circles and open diamonds).

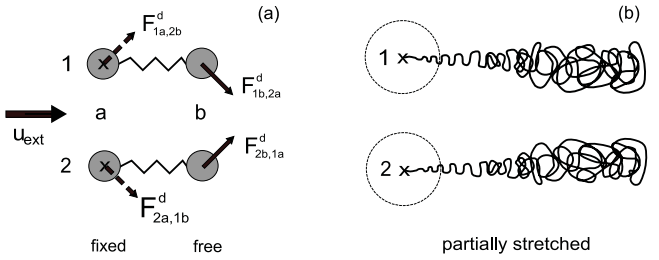

FIG. 3. (a) Illustration of the polymer-polymer attraction for two toy chains consisting of two beads a and b connected by springs. The HI between beads a and b belonging to different chains induces lateral drag forces F^d along the y axis by which the chains attract each other. (b) For larger polymer chains the HI between the many beads leads to an inward motion of the chains, and they approach each other.

of mass (com) of the two chains. If the chains do not interact, $D_{\rm sep} - \Delta y_{\rm com}$ must vanish since no lateral forces exist that could cause a lateral displacement. However, when HI is significant, $D_{\rm sep} - \Delta y_{\rm com}$ is positive (see dashed lines in Fig. 2), implying that the two chains attract each other. As expected, with smaller separation of the tether points $D_{\rm sep}$, the attraction is larger since the interchain HI is enhanced. With increasing flow $u_{\rm ext}/u_{\rm ref}$ the lateral displacement of the polymers decreases as the longitudinal drag in flow direction starts to dominate the lateral attractive force.

The basic mechanism of the chain attraction can be understood by considering a simple model consisting of two chains 1 and 2 with two beads, a and b. The a beads are hooked to a tether point, as indicated by a cross in Fig. 3(a). When a uniform flow $u_{\rm ext}\hat{e}_x > 0$ is imposed, the fluid exerts a drag force on all four beads pointing along the positive x axis. To keep all beads in place, the flow-induced drag must be counterbalanced by constraint forces $\mathbf{F}^{dir}$ pointing along the negative x axis, which are the source for a flow perturbation via $\mathbf{v} = \mathbf{H} \cdot \mathbf{F}^{dir}$. To obtain the effective flow field seen by each bead, $\mathbf{v}$ needs to be superposed to the unperturbed flow $u_{\rm ext}\hat{e}_x$, so that the total flow field is given by $u_{\rm ext}\hat{e}_x + \mathbf{H} \cdot \mathbf{F}^{dir}$. To determine the perturbation $\mathbf{v}$, we assume for simplicity that the beads are pointlike, in which case the mobility matrix is given by the Oseen tensor $\mathbf{H}_{i,j} = 1/8\pi\eta r_{i,j}\left[\mathbf{I} + \hat{\mathbf{r}}_{i,j} \otimes \hat{\mathbf{r}}_{i,j}\right]$. In the following, we consider the case where F_x^{dir} acts on bead $1a$ and determine the perturbed flow at bead $2b$, i.e., $\mathbf{v}_{2b} = \mathbf{H}_{2b,1a} \cdot \mathbf{F}_{1a}^{dir}$. With bead $1a$ at the origin $\mathbf{R}_{1a} = (0,0)$ and bead $2b$ positioned at $\mathbf{R}_{2b} = (d_x, -d_y)$, their distance vector reads $\mathbf{r}_{2b,1a} = (d_x, -d_y)$. Inserting the x and y components of $\mathbf{r}_{2b,1a}$ into the Oseen tensor, one obtains $v_{2b}^x \propto \left[1 + d_x^2\right] F_x^{dir}$ and $v_{2b}^y \propto -d_x d_y F_x^{dir}$. Since $F_x^{dir} < 0$, it follows that $v_{2b}^x < 0$ and $v_{2b}^y > 0$. Adding these latter flow components to $u_{\rm ext}\hat{e}_x > 0$ leads to the effective flow field and drag force $F_{2b,1a}^d$ at the position of bead $2b$, as shown in Fig. 3(a).

A similar analysis can be applied to all other beads and results in the HI-induced effective local drag forces illustrated in Fig. 3(a). Since the a beads are bound to the tether points while the b beads can move more freely, chains 1 and 2 perform an inward motion and approach each other. The same basic mechanism applies to longer chains, as sketched in Fig. 3(b). Note that the lateral drag forces derived are only *nonzero* if the distance vector $\mathbf{r}_{i,j}$ is *skewly* oriented to the flow direction determined by $u_{\rm ext}\hat{e}_x$, so that bead pairs (i,j) whose vector $\mathbf{r}_{i,j}$ is either parallel $[(1a,1b), (2a,2b)]$ or perpendicular $[(1a,2a), (1b,2b)]$ to the flow direction do not contribute to any lateral drag. The analysis so far has considered the initial situation, where the toy chains are exactly aligned with the flow direction. The HI-induced lateral forces then move the b beads inward up to a certain angle, so that the final orientation of the two chains as given, e.g., by their connector vector $\mathbf{r}_{ia,ib}$ $i = 1,2$ is skewed relative to the flow axis. The magnitude of this angle depends on the distance between the a beads and the length of the spring between the a and b beads.

If we now turn on thermal fluctuations ($T > 0$), the polymer adopts a partially coiled conformation, which is determined by the force balance between the restoring entropic force and the external drag. As shown in Fig. 2 (solid lines), for larger velocities $u_{\rm ext}/u_{\rm ref} > 5$ the chain attraction is only slightly larger than without fluctuations, while at small velocities, depending on $D_{\rm sep}$, the attraction is somewhat weaker with than without fluctuations. Within an intermediate velocity regime $1 < u_{\rm ext}/u_{\rm ref} < 5$, the attraction is strongly enhanced. We can understand this fluctuation-induced enhancement of the polymer-polymer attraction by considering that at small and intermediate flow velocities the polymers are still in a rather coiled state, so that larger portions of the polymer are quite close, with a mutual distance smaller than $D_{\rm sep}$. Since the HI behaves as $1/r$, the chain sections closer to each other interact more strongly, which results in an enhanced polymer-polymer attraction at intermediate flow velocities. With increasing flow $u_{\rm ext}/u_{\rm ref}$ the chains become more and more elongated, while their mutual distance grows. Again, as HI decays as $1/r$, the interchain HI is now weaker than in the (partially) coiled state, so that the polymer attraction falls off, as shown in Fig. 2.

Note that when the distance between the tether points is reduced further, the interchain EVI becomes important at some lower critical value of $D_{\rm sep}$. In this case, one expects that the

HI-induced lateral force is compensated by the repulsive EVI, so that the maximum of the lateral displacement should be less pronounced. The fact that $D_{\mathrm{sep}} - \Delta y_{\mathrm{com}}$ for the distance $D_{\mathrm{sep}} = 10$ is larger than for $D_{\mathrm{sep}} = 20$ indicates that one has not reached this lower critical value where the interchain EVI would play a role. Finally, if EVI were discarded entirely, the lateral displacements would be lower, specifically within intermediate velocities $1 \leqslant u_{\mathrm{ext}}/u_{\mathrm{ref}} \leqslant 5$, where the polymer is partially coiled. This is because without EVI the polymer's size (given, e.g., by its radius of gyration) is smaller than with EVI, so that the distance between the beads of different chains is larger and results in a reduction of the interchain HI. The exclusion of EVI, however, should not affect the qualitative behavior shown in Fig. 2(b).

In summary, we investigated hydrodynamic interaction effects in tethered polymers exposed to a uniform flow by means of Brownian dynamics simulations and considered two settings. It was shown that a unique identification of HI effects is possible by measuring the drag coefficient of a polymer in uniform flow, which becomes dependent on the flow velocity only if HI is significant. In this case, the velocity-dependent drag force may be interpreted as a nonlinear generalization of the Stokes' law for a rigid sphere. Further, we have demonstrated that HI not only causes intrachain screening but also mediates an interaction between different chains. This interchain screening leads to a further reduction of the drag per polymer as well as to an effective attractive lateral force, whose presence can be detected by measuring the lateral polymer's displacement. The polymer attraction shows a pronounced maximum in a velocity range where the drag forces are of the order of the entropic forces. The suggested setups used in the simulations are suitable for experiments, where these HI effects may be probed for real polymers, as we propose.

This work was supported by the German Science Foundation via the priority program SPP1164 and SFB840.

[1] P. G. deGennes, *Scaling Concepts in Polymer Physics* (Cornell University Press, Ithaka, NY, 1979).
[2] R. Bird, C. Curtiss, R. Armstrong, and O. Hassager, *Dynamics of Polymeric Liquids I* (Wiley, New York, 1987).
[3] A. Gyr and H. W. Bewersdorff, *Drag Reduction of Turbulent Flows by Additives* (Kluwer, Dordrecht, 1995).
[4] A. Groisman and V. Steinberg, Nature (London) **405**, 53 (2000).
[5] P. G. De Gennes, J. Chem. Phys. **60**, 5030 (1974).
[6] T. T. Perkins, D. E. Smith, R. G. Larson, and S. Chu, Science **268**, 83 (1995).
[7] T. T. Perkins, D. E. Smith, and S. Chu, Science **276**, 2016 (1997).
[8] D. E. Smith, H. P. Babcock, and S. Chu, Science **283**, 1724 (1999).
[9] P. LeDuc, C. Harber, G. Bao, and D. Wirtz, Nature (London) **399**, 564 (1999).
[10] C. M. Schroeder, H. P. Babcock, E. S. G. Shaqfeh, and S. Chu, Science **301**, 1515 (2003).
[11] P. S. Doyle, B. Ladoux, and J. L. Viovy, Phys. Rev. Lett. **84**, 4769 (2000); B. Ladoux and P. S. Doyle, Europhys. Lett. **52**, 511 (2000).
[12] M. A. Webster and J. M. Yeomans, J. Chem. Phys. **122**, 164903 (2005).
[13] R. Delgado Buscalioni, Phys. Rev. Lett. **96**, 088303 (2006).
[14] P. Szymczak and M. Cieplak, J. Chem. Phys. **127**, 155106 (2007).
[15] C. A. Lueth and E. S. G. Shaqfeh, Macromolecules **42**, 9170 (2009).
[16] Y. Zhang, A. Donev, T. Weisgraber, B. J. Adler, M. D. Graham, and J. J. de Pablo, J. Chem. Phys. **130**, 234902 (2009).
[17] F. Brochard-Wyart, Europhys. Lett. **23**, 105 (1993); **30**, 387 (1995).
[18] R. G. Larson, T. T. Perkins, D. E. Smith, and S. Chu, Phys. Rev. E **55**, 1794 (1997).
[19] R. Rzehak, D. Kienle, T. Kawakatsu, and W. Zimmermann, Europhys. Lett. **46**, 821 (1999).
[20] R. Rzehak, W. Kromen, T. Kawakatsu, and W. Zimmermann, Eur. Phys. J. E **2**, 3 (2000).
[21] D. Kienle and W. Zimmermann, Macromolecules **34**, 9173 (2001).
[22] P. Szymczak and M. Cieplak, J. Chem. Phys. **125**, 164903 (2006).
[23] B. H. Zimm, Macromolecules **31**, 6089 (1998).
[24] D. Stigter and C. Bustamante, Biophys. J. **75**, 1197 (1998).
[25] D. L. Ermak and J. A. McCammon, J. Chem. Phys. **69**, 1352 (1978).
[26] M. Fixman, Macromolecules **19**, 1204 (1986).
[27] H. R. J. Warner, Ind. Eng. Chem. Fundam. **11**, 379 (1972).
[28] G. S. Grest and K. Kremer, Phys. Rev. A **33**, 3628 (1986).
[29] J. Rotne and S. Prager, J. Chem. Phys. **50**, 4831 (1969).
[30] G. Goldmann, R. Cox, and H. Brenner, Chem. Eng. Sci. **21**, 1151 (1966).
[31] L. D. Landau and E. M. Lifshitz, *Lehrbuch der Theoretischen Physik* (Wiley, New York, 1987), Vol. 6.